

# Full Wave Analysis of MHD Modes Using Multi-Fluid Dielectric Tensor in an Inhomogeneous Plasma

AKUTSU Taku and FUKUYAMA Atsushi

*Department of Nuclear Engineering, Kyoto University, Kyoto 606-8501, Japan*

(Received: 9 December 2003 / Accepted: 26 February 2004)

## Abstract

Analysis of linear stability of plasmas by solving Maxwell's equations using dielectric tensor is described. Dielectric tensor is derived from multi-fluid equations taking the electron inertia, the pressure gradient, the parallel current, and the collisional friction into account. Numerical calculations using a newly developed numerical code TASK/WA illustrate the effect of pressure gradient on the TAE (Toroidicity-induced Alfvén Eigenmode) [1] and the pressure dependence of the internal kink mode.

## Keywords:

dielectric tensor, wave analysis, multi-fluid, TAE, internal kink mode

## 1. Introduction

Macroscopic instabilities of plasmas are important subjects in fusion research and have been extensively studied by use of magnetohydrodynamics. In a high temperature plasma, however, kinetic effects play a vital role in stabilizing and destabilizing plasmas. In most of previous analyses, kinetic effects are involved perturbatively. To take the kinetic effects into account non-perturbatively, we solve Maxwell's equations using dielectric tensor which expresses the linear response of plasmas. Dielectric tensor can be derived for different physics models such as multi-fluid model, kinetic model (without drift motion), drift kinetic model, drift kinetic model taking account of particle orbit, and so on.

In this paper, as a first step, we employ a dielectric tensor derived from the collisional multi-fluid equations taking the electron inertia, the pressure gradient, and the parallel current into account. The numerical results for tokamak plasmas illustrate the effect of pressure gradient on the TAE and the pressure dependence of the internal kink mode [2].

## 2. Full wave analysis of eigenmode

We solve Maxwell's equations for the scalar  $\phi$  and vector potential  $\mathbf{A}$  in the flux coordinates  $(\alpha, \beta, \varphi)$

$$-\nabla \times \nabla \times \mathbf{A} + \frac{i\omega}{c^2} \vec{\epsilon} \cdot \nabla \phi + \frac{\omega^2}{c^2} \vec{\epsilon} \cdot \mathbf{A} = -\mu_0 \mathbf{j}_{ext} \quad (1)$$

$$\nabla \cdot \vec{\epsilon} \cdot \nabla \phi - i\omega \nabla \cdot \vec{\epsilon} \cdot \mathbf{A} = \frac{i}{\omega \epsilon_0} \nabla \cdot \mathbf{j}_{ext} \quad (2)$$

$$\nabla \cdot \mathbf{A} = 0 \quad (3)$$

where  $\vec{\epsilon}$  is the dielectric tensor,  $\alpha$ ,  $\beta$  and  $\varphi$  are the toroidal

flux, poloidal angle, and toroidal angle respectively. Other notations are standard. Then, we obtain eigen functions and eigen frequencies by searching for the complex frequencies which make the wave electric field maximum for a given external current  $\mathbf{j}_{ext}$  proportional to the plasma density [3].

## 3. Derivation of dielectric tensor from multi-fluid equations

We derive a dielectric tensor by linearizing the multi-fluid equations (equations of continuity, motion, and state):

$$\frac{\partial n_j}{\partial t} + \nabla \cdot (n_j \mathbf{u}_j) = 0 \quad (4)$$

$$m_j n_j \left( \frac{\partial}{\partial t} + \mathbf{u}_j \cdot \nabla \right) \mathbf{u}_j = -\nabla P_j + q_j n_j (\mathbf{E} + \mathbf{u}_j \times \mathbf{B}) - n_j \sum_{k \neq j} \langle \sigma v \rangle_{jk} (\mathbf{u}_j - \mathbf{u}_k) \quad (5)$$

$$\frac{d}{dt} (P_j n_j^{-\gamma}) = 0 \quad (6)$$

where  $m_j$ ,  $q_j$ ,  $n_j$ ,  $\mathbf{u}_j$ ,  $P_j$  are the mass, charge, density, fluid velocity and pressure of the particle species  $j$ ,  $\mathbf{E}$  is the electric field,  $\mathbf{B}$  is the magnetic field, and  $\langle \sigma v \rangle_{jk}$  is the collision rate between the particle species  $j$  and  $k$ . The multi-fluid equations are solved with respect to the first order particle flux  $\Gamma_{j1} = n_{j0} \mathbf{u}_{j1} + n_{j1} \mathbf{u}_{j0}$ , and a conductivity tensor  $\vec{\sigma}$  is derived by substituting  $\Gamma_{j1}$  to the equation  $\mathbf{j}_1 = \sum_j q_j \Gamma_{j1} = \sum_j \vec{\sigma}_j \cdot \mathbf{E}$ . Then, dielectric tensor is calculated from

$$\vec{\epsilon} = \vec{I} + \sum_j \frac{i}{\omega \epsilon_0} \vec{\sigma}_j. \quad (7)$$

For simplicity, we define local orthogonal coordinates, derive the dielectric tensor on them, and transform it for the flux coordinates. The definitions of the local orthogonal coordinates are

$$\hat{x} = \nabla\alpha/|\nabla\alpha|, \quad \hat{z} = \mathbf{B}_0/B_0, \quad \hat{y} = \hat{z} \times \hat{x} \quad (8)$$

and transformation is expressed by

$$\vec{\epsilon}_{flux} = \vec{\mu} \cdot \vec{\epsilon}_{xyz} \cdot \vec{\mu}^{-1} \quad (9)$$

where

$$\vec{\mu} = \begin{pmatrix} \hat{x} \cdot \nabla\alpha & \hat{x} \cdot \nabla\beta & \hat{x} \cdot \nabla\varphi \\ \hat{y} \cdot \nabla\alpha & \hat{y} \cdot \nabla\beta & \hat{y} \cdot \nabla\varphi \\ \hat{z} \cdot \nabla\alpha & \hat{z} \cdot \nabla\beta & \hat{z} \cdot \nabla\varphi \end{pmatrix}. \quad (10)$$

The conductivity tensor  $\vec{\sigma}_{j,xyz}$  of each particle species in local orthogonal coordinates satisfies following relations.

$$\begin{pmatrix} \vec{I} & \vec{X}_{ie} \\ \vec{X}_{ei} & \vec{I} \end{pmatrix} \begin{pmatrix} \vec{\sigma}_{i,xyz} \\ \vec{\sigma}_{e,xyz} \end{pmatrix} = \begin{pmatrix} \vec{\sigma}_{0i} \\ \vec{\sigma}_{0e} \end{pmatrix} \quad (11)$$

where the subscripts  $i$  and  $e$  denote ion and electron, respectively, and

$$\vec{\sigma}_{0j} = \frac{iq_j^2 n_{j0}}{m_j} \vec{C}_j \cdot \left( \vec{I} + \frac{1}{\omega} \mathbf{u}_{j0} \times \mathbf{k} \right) \quad (12)$$

$$\vec{X}_{jk} = -in_{j0} \frac{q_k}{q_j} \vec{C}_j \cdot \left( \vec{I} - \frac{\mathbf{u}_{j0} \mathbf{k}}{\omega} \right) \langle \sigma v \rangle_{jk} \quad (13)$$

$$\vec{C}_j = \frac{\vec{M}_j}{(\omega'_j + iv_j)} \cdot \left[ \vec{I} + \frac{\gamma T_j}{m_j \omega W_j} \mathbf{k}' \cdot \mathbf{k} \cdot \vec{M}_j \right] \quad (14)$$

$$W_j = \omega'_j + iv_j - \frac{\gamma T_j}{m_j \omega} \mathbf{k} \cdot \vec{M}_j \cdot \mathbf{k}' \quad (15)$$

$$\vec{M}_j = \delta^{-1}$$

$$\times \begin{pmatrix} (\omega'_j + iv_j)^2 & i\Omega_j (\omega'_j + iv_j) & 0 \\ -i(\Omega_j + u'_{j0y} - Z_j k_y)(\omega'_j + iv_j) & (\omega'_j + iv_j)(\omega'_j + iv_j - iZ_j k_x) & 0 \\ -i(u'_{j0z} - Z_j k_z)(\omega'_j + iv_j) & \Omega_j (u'_{j0z} - Z_j k_z) & \delta \end{pmatrix} \quad (16)$$

$$\delta = (\omega'_j + iv_j)(\omega'_j + iv_j - iZ_j k_x) - \Omega_j (\Omega_j + u'_{j0y} - Z_j k_y) \quad (17)$$

$$\Omega_j = q_j B_0 / m_j \quad (18)$$

$$Z_j = \frac{1}{m_j n_{j0} \omega'_j} \left( \gamma T_{j0} \frac{dn_{j0}}{dx} - \frac{dP_{j0}}{dx} \right) \quad (19)$$

$$v_j = \sum_{k \neq j} n_{k0} \langle \sigma v \rangle_{jk} \quad (20)$$

$$\omega'_j = \omega - \mathbf{k} \cdot \mathbf{u}_{j0} \quad (21)$$

$$\gamma T_j \mathbf{k}' = \gamma T_j \mathbf{k} + \omega'_j m_j \mathbf{u}_{j0} + iq_j E_0 + im_j \sum_{k \neq j} \langle \sigma v \rangle_{jk} n_{k0} \mathbf{u}_{k0} \quad (22)$$

In the collisionless limit,  $\langle \sigma v \rangle_{jk} \rightarrow 0$ ,  $\vec{\sigma}_{j,xyz} = \vec{\sigma}_{0j}$ .

## 4. Numerical calculations

We have developed a new numerical code TASK/WA to solve Maxwell's equations. TASK/WA uses the finite difference method in the  $\alpha$  direction, and Fourier decomposition in the  $\beta$  and  $\varphi$  directions. In the present calculations, a circular cross section ( $R - R_0 = \rho \cos \beta$ ,  $Z = \rho \sin \beta$ ,  $\rho = \sqrt{\alpha/\alpha_{max}}$ ) is assumed, and the density profile, temperature profile, and  $q$  profile are given by

$$n_j = (n_{j0} - n_{ja}) (1 - \rho^2) + n_{ja} \quad (23)$$

$$T_j = (T_{j0} - T_{ja}) (1 - \rho^2) + T_{ja} \quad (24)$$

$$q = q_0 + (q_a - q_0) \rho^2 \quad (25)$$

Other parameters are as follows: toroidal mode number  $n = 1$ ,  $B_0 = 3$  T,  $R_0 = 3$  m,  $a = 1$  m,  $n_{e0} = 10^{20}$  m $^{-3}$ ,  $n_{ea} = 10^{10}$  m $^{-3}$ ,  $T_{e0} = 3$  keV,  $T_{ea} = 1$  eV,  $\langle \sigma v \rangle_{ei} \propto Z^2 T_j^{-3/2}$ .

### 4.1 Analysis in the frequency range of TAE and the lower

We studied the effects of the pressure gradient, parallel current, and collisions on TAE and other low frequency modes with  $q_0 = 1$  and  $q_a = 2$ . Figure 1(a) ~ (d) are contour plots of  $[\log(\int |\mathbf{E}|^2 dV)]^{-1}$  as a function of complex frequency  $f$ , where  $\mathbf{E} = -\nabla\phi + i\omega\mathbf{A}$  is the wave electric field to be integrated over the plasma volume. The darker the color becomes, the larger the wave electric field is. Figure 1(a) is a reference case (without the pressure gradient, parallel current, and collisions). The hollow point of  $f \approx 0.165$  MHz is TAE. With the pressure gradient, new two branches appears in the region of  $\text{Re}(f) < 0.1$  MHz (Fig. 1(b)). Because the effects of continuum damping and radiative damping are not included in the dielectric tensor, the damping rate of TAE without pressure gradient, parallel current, and collisions is nearly 0. And with pressure gradient, the mode distribution is symmetric with respect to the real axis. With pressure gradient

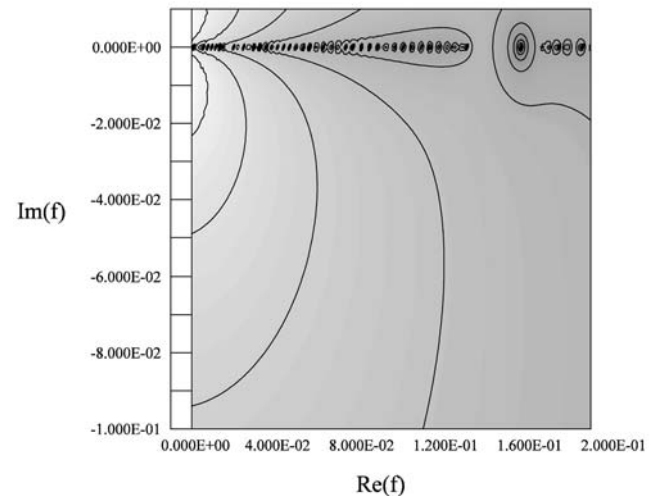


Fig. 1(a) Contour map of  $[\log(\int |\mathbf{E}|^2 dV)]^{-1}$  as a function of complex frequency for TAE or low frequency modes without pressure gradient, parallel current and collisions ( $q_0 = 1$ ,  $q_a = 2$ ).

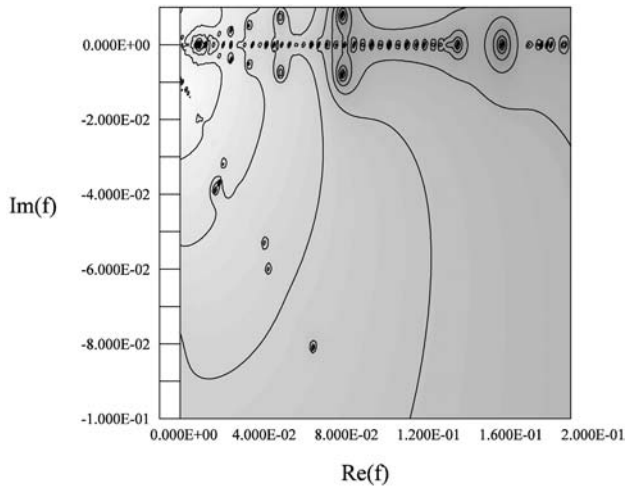


Fig. 1(b) with pressure gradient, without parallel current and collisions

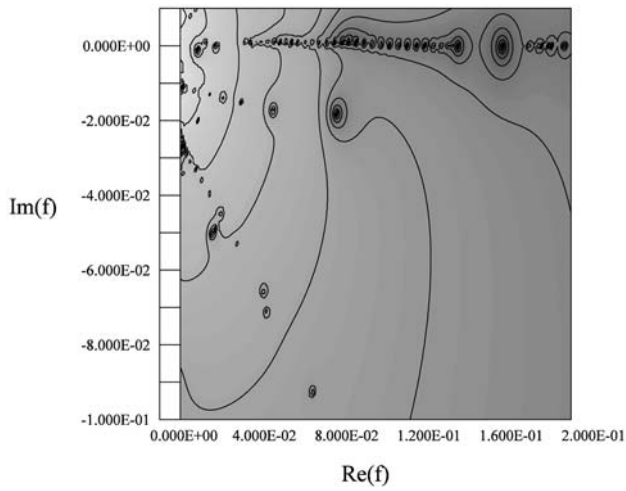


Fig. 1(c) with pressure gradient and collisions, without parallel current

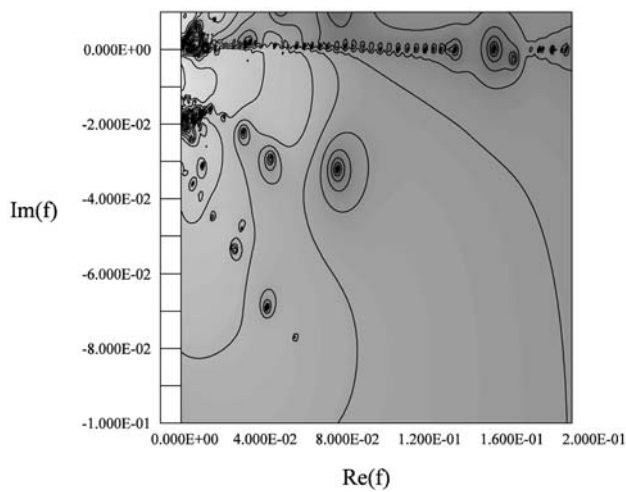


Fig. 1(d) with collisions, pressure gradient and parallel current

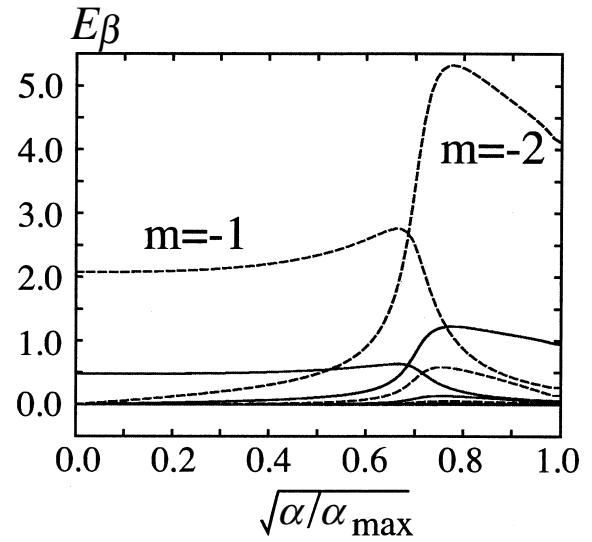


Fig. 2(a) TAE mode structure ( $E_\beta$ ) without pressure gradient, parallel current and collisions

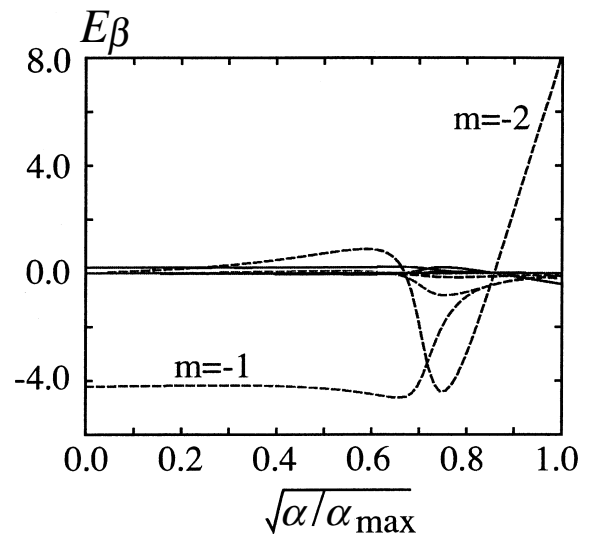


Fig. 2(b) With pressure gradient, without parallel current and collisions

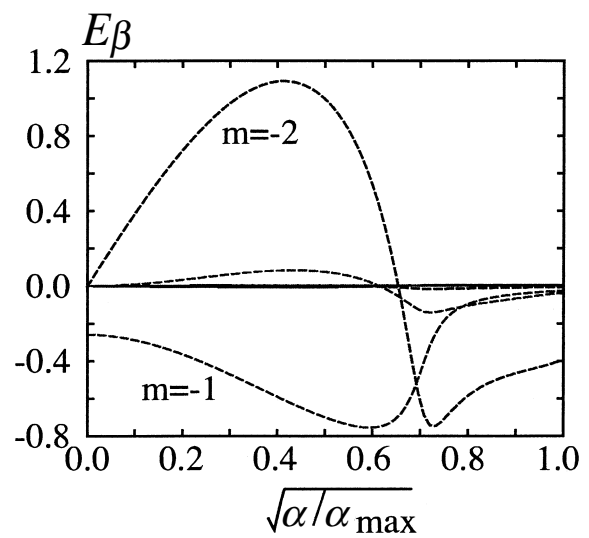


Fig. 2(c) With parallel current, without pressure gradient and collisions

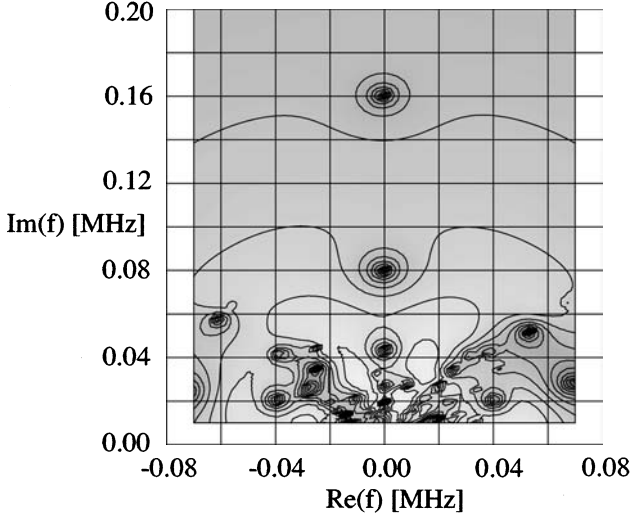


Fig. 3 Contour map of  $[\log(|E|^2 dV)]^{-1}$  as a function of complex frequency for internal kink mode ( $q_0 = 0.7$ ,  $q_a = 3$ )

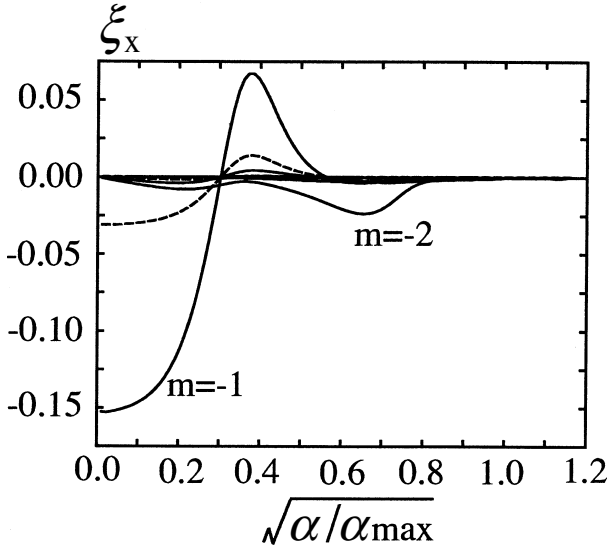


Fig. 4 Displacement in x-direction for internal kink mode ( $q_0 = 0.7$ ,  $q_a = 3$ )

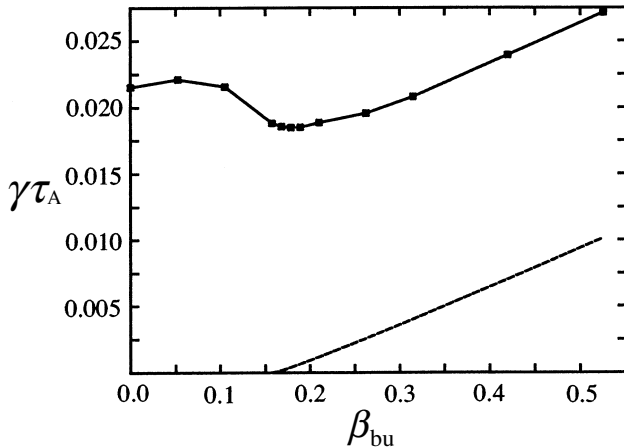


Fig. 5 Growth rate of internal kink mode as a function of  $\beta_{bu}$ . Growth rate obtained by TASK/WA (solid line) and Eq. (26) (dotted line).

and collisions, asymmetry of mode distribution becomes dominant and unstable mode disappears (Fig. 1(c)). Parallel current does not make large effects on the modes distribution in the complex frequency space (Fig. 1(d)).

The effects of the pressure gradient, parallel current, and collisions on TAE radial mode structure are shown in Fig. 2(a) ~ (c). With parallel current,  $m = -2$  electric field becomes larger compared with other cases.

## 4.2 Analysis of internal kink mode

Internal kink mode is analysed with  $q_0 = 0.7$  and  $q_a = 3$ . In Fig. 3, the internal kink mode corresponds to the hollow point in  $f \approx 0.08i$  MHz. And the displacement of the mode is shown in Fig. 4.

In Fig. 5, the dependence of the internal kink growth rate  $\gamma$  on pressure is compared with the formula obtained by An. Martynov *et al.* [4]:

$$\gamma\tau_A = 0.5\varepsilon_1(\kappa_1 - 0.5) \times \left( \beta_{bu} - \left( 0.5 - \frac{\varepsilon_1}{\varepsilon_a} (\kappa_1 - 1.5|\delta_1 + 0.04|) \right) \right)^{(1.23 - 1.26\varepsilon_1)} \quad (26)$$

where  $\tau_A$  is the Alfvén time,  $\beta_{bu} = 2\mu_0(\langle p \rangle_1 - p_1)/B_{pl}^2$  is the so-called beta Bussac,  $\langle p \rangle_1$  is the volume-averaged pressure over the inside of the  $q = 1$  surface,  $p_1$ ,  $B_{pl}$ ,  $\varepsilon_1$ ,  $\kappa_1$ ,  $\delta_1$  are the pressure, poloidal magnetic field, inverse aspect ratio, elongation, and triangularity on  $q = 1$  surface.  $\varepsilon_a$  is the inverse aspect ratio on plasma edge. In the present calculations,  $\varepsilon_1 = 0.12$ ,  $\varepsilon_a = 0.33$ ,  $\kappa_1 = 1$ , and  $\delta_1 = 0$ . Though the slope of growth rates obtained by TASK/WA is coincident with Eq. (26), and the minimum point of TASK/WA ( $\beta_{bu} = 0.168$ ) is almost coincident with 0.161 obtained from Eq. (26),  $\gamma\tau_A$  differs by about 0.017 for wide range of  $\beta_{bu}$ . This discrepancy may be attributed to the other destabilizing mechanism such as parallel current, but not yet understood well.

## 5. Conclusions

We derived the dielectric tensor including the effects of pressure gradient, the parallel current, and the collisional friction.

These effects in the TAE and the lower frequency region are investigated using the code TASK/WA. With pressure gradient, two new symmetric branches appear in the region of  $\text{Re}(f) < 0.1$  MHz (Fig. 1(b)). Because the effects of continuum damping and radiative damping are not included in the dielectric tensor, quantitative analyses of the damping rate is out range of the present study.

While the parallel current does not make large effects on the mode distribution in the complex frequency space, mode structure is strongly affected and  $m = -2$  electric field becomes larger compared with the cases without the parallel current.

The growth rate of the internal kink mode obtained by TASK/WA is compared with the previous computation result Eq. (26). The relative dependence of the growth rate on the pressure  $\beta_{bu}$  agrees well with each other, but the positive offset of the growth rate may be attributed to some destabilizing

mechanism such as parallel current, which is left for further study.

### References

- [1] C.Z. Cheng, Liu Chen and M.S. Chance, *Ann. of Phys.* **161**, 21 (1985).
- [2] J.A. Wesson, *Nucl. Fusion* **18**, 87 (1978).
- [3] A. Fukuyama and T. Akutsu, *Proc. of IAEA Fusion Energy Conference* (Lyon, France) IAEA-CN-94/TH/P3-14.
- [4] An. Martynov and O. Sauter, *Proc. Joint Varenna-Lausanne Int. Workshop* (Varenna 2002) p. 297.